THE JOURNAL OF BIOLOGICAL CHEMISTRY VOL. 287, NO. 34, pp. 28609–28618, August 17, 2012

Kinetic Analysis of DNA Strand Joining by *Chlorella* Virus DNA Ligase and the Role of Nucleotidyltransferase Motif VI in Ligase Adenylylation*[S]

Received for publication, May 10, 2012, and in revised form, June 7, 2012 Published, JBC Papers in Press, June 28, 2012, DOI 10.1074/jbc.M112.380428

Poulami Samai and Stewart Shuman[1]

From the Molecular Biology Program, Sloan-Kettering Institute, New York, New York 10065

Background: DNA ligases play essential roles in DNA replication, recombination, and repair.
Results: Rapid mix-quench methods reveal the kinetic mechanism of nick sealing by a eukaryal ATP-dependent DNA ligase.
Conclusion: The rate-limiting step in ligase catalysis changes as a function of pH.
Significance: Structure-guided mutagenesis and kinetic analysis underscore distinctive enzymic requirements for the three chemical steps of the ligation pathway.

***Chlorella* virus DNA ligase (ChVLig) is an instructive model for mechanistic studies of the ATP-dependent DNA ligase family. ChVLig seals 3′-OH and 5′-PO_4 termini via three chemical steps: 1) ligase attacks the ATP α phosphorus to release PP_i and form a covalent ligase-adenylate intermediate; 2) AMP is transferred to the nick 5′-phosphate to form DNA-adenylate; 3) the 3′-OH of the nick attacks DNA-adenylate to join the polynucleotides and release AMP. Each chemical step requires Mg^{2+}. Kinetic analysis of nick sealing by ChVLig-AMP revealed that the rate constant for phosphodiester synthesis ($k_{step3} = 25\ s^{-1}$) exceeds that for DNA adenylylation ($k_{step2} = 2.4\ s^{-1}$) and that Mg^{2+} binds with similar affinity during step 2 ($K_d = 0.77$ mM) and step 3 ($K_d = 0.87$ mM). The rates of DNA adenylylation and phosphodiester synthesis respond differently to pH, such that step 3 becomes rate-limiting at pH ≤ 6.5. The pH profiles suggest involvement of one and two protonation-sensitive functional groups in catalysis of steps 2 and 3, respectively. We suggest that the 5′-phosphate of the nick is the relevant protonation-sensitive moiety and that a dianionic 5′-phosphate is necessary for productive step 2 catalysis. Motif VI, located at the C terminus of the OB-fold domain of ChVLig, is a conserved feature of ATP-dependent DNA ligases and GTP-dependent mRNA capping enzymes. Presteady state and burst kinetic analysis of the effects of deletion and missense mutations highlight the catalytic contributions of ChVLig motif VI, especially the Asp-297 carboxylate, exclusively during the ligase adenylylation step.**

ATP-dependent DNA ligases are ubiquitous in archaea and eukarya and are widely prevalent in bacteria and viruses (1). Their functions encompass Okazaki fragment joining, nucleotide and base excision repair, homologous recombination, and nonhomologous end joining (2). *Chlorella* virus DNA ligase (ChVLig)[2] is a minimized (298-amino acid) eukaryal enzyme that has proved to be an instructive model for structural and mechanistic studies of the ATP-dependent ligase family (3–8).

ChVLig consists of three structural domains, nucleotidyltransferase (NTase), OB-fold, and latch, which envelop the nicked DNA as a C-shaped protein clamp (see Fig. 1*A*) (8). The N-terminal NTase domain (amino acids 1–189), which performs the chemical steps of ligation, binds the major groove flanking the nick and the minor groove on the 3′-OH side of the nick (see Fig. 1*A*). The NTase active site is composed of a cage of β strands and interstrand loops that include six peptide motifs (I, Ia, III, IIIa, IV, and V) that define the covalent nucleotidyltransferase superfamily (DNA ligases, RNA ligases, and mRNA capping enzymes) (9). Motif I (^{25}TPKIDGIR^{32} in ChVLig) contains the lysine (Lys-27) to which AMP becomes covalently linked in the first step of the DNA ligase reaction (see Fig. 1*B*) (6). Amino acids in motifs I, Ia, III, IIIa, IV, and V contact AMP or the DNA nick and play essential roles in the ligation pathway (see Fig. 1*B*) (4–6, 10–13).

The C-terminal OB domain of ChVLig, composed of a five-strand antiparallel β barrel and an α helix, engages the DNA minor groove on the face of the duplex behind the nick (see Fig. 1*A*). The OB domain also makes functionally important contacts to amino acids in the NTase domain surrounding the ligase active site, *e.g.* the salt bridge from Arg-285 in the OB domain to Asp-29 in motif I of the NTase domain (see Fig. 1*B*) (13). The latch module, consisting of a β hairpin loop (amino acids 203–231) that emanates from the OB domain, occupies the DNA major groove flanking the nick. Residues at the tip of the latch contact the NTase domain to close the ligase clamp.

An extensive structure-guided mutational analysis of ChVLig has illuminated the contributions of the amino acid side chains that (i) directly promote catalysis of one or more of the chemical steps in the ligation pathway; (ii) comprise the extended ligase DNA footprint and make atomic contacts with the 3′-OH and 5′-phosphate strands or the continuous template strand; (iii) elicit conformational distortion of the DNA in

* This work was supported, in whole or in part, by National Institutes of Health Grant GM63611.
[S] This article contains supplemental Tables S1–S3 and Figs. S1–S5.
[1] An American Cancer Society Research Professor. To whom correspondence should be addressed. E-mail: s-shuman@ski.mskcc.org.

[2] The abbreviations used are: ChVLig, *Chlorella* virus DNA ligase; NTase, nucleotidyltransferase; HuLig1, human DNA ligase I.

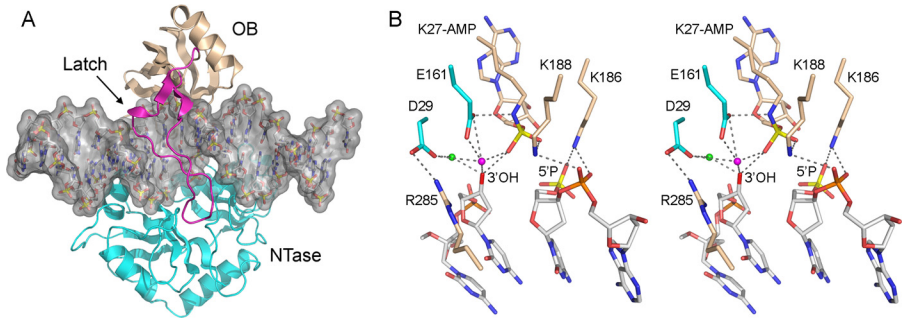

FIGURE 1. **Structure and active site of ChVLig-AMP bound to nicked DNA.** *A*, ChVLig-AMP is shown as a ribbon trace bound to nicked DNA, which is rendered as transparent surface over a stick model (Protein Data Bank code 2Q2T). The ChVLig NTase, OB, and latch domains are colored *cyan*, *beige*, and *magenta*, respectively. *B*, Stereo view of the active site of ChVLig-AMP bound at a nick. The terminal dinucleotides of the 3′-OH and 5′-phosphate strands are shown as stick models with *gray* carbons. Atomic contacts to the lysyl-AMP, the nick 3′-OH, 5′-phosphate, and penultimate phosphodiester are depicted as *dashed lines*. Two waters are depicted as *green* and *magenta* spheres. The water proposed to mimic a catalytic Mg^{2+} is colored *magenta*. The metal-binding Asp-29 (motif I) and Glu-161 (motif IV) side chains are highlighted as stick models with *cyan* carbons.

the vicinity of the nick; and (iv) form or stabilize the ligase clamp. Such studies have employed *in vivo* and *in vitro* readouts of the composite ChVLig nick sealing activity, plus biochemical assays of isolated steps in the ligase pathway (3–14).

A recent innovation to the functional analysis of DNA ligation is the application of rapid mix-quench methods to study the transient state kinetics of nick sealing by preformed ligase-adenylate (13–16). As implemented for ChVLig (13, 14), the observed rate profiles fit well to a unidirectional scheme of DNA adenylylation (step 2, Lig-AMP·pDNA → Lig·AppDNA) and subsequent phosphodiester synthesis (step 3, Lig·AppDNA → Lig·AMP·DNApDNA), with allowance for reversible branching of Lig·AppDNA to an "out-of-pathway" state (*e.g.* Lig + AppDNA) (13). The observed step 2 and step 3 rate constants (k_{step2} and k_{step3}) for wild-type ChVLig were 2.4 s^{-1} and 24 s^{-1}, respectively (14). Thus, the attack of the nick 3′-OH on AppDNA is an order of magnitude faster than the formation of AppDNA. Similar single-turnover kinetic studies have been performed for human DNA ligase I (HuLig1) (15) and bacteriophage T4 DNA ligase (16), yielding rate constants as follows: HuLig1 (k_{step2} 2.6 s^{-1}; k_{step3} 12 s^{-1}) and bacteriophage T4 DNA ligase (k_{step2} 5.3 s^{-1}; k_{step3} 38 s^{-1}). It would appear that diverse ATP-dependent DNA ligases have similar kinetic properties with respect to steps 2 and 3. Kinetic analysis of nick sealing by a large collection of ChVLig mutants revealed the quantitative contributions of individual functional groups to step 2 and step 3 catalysis and, in some instances, a selective negative impact of mutations on step 3 *versus* step 2 or vice versa (11, 13, 14).

The aims of the present study were two-fold. First, we sought to determine the effects of varying the divalent cation concentration and the pH on the rates of steps 2 and 3 and thereby gain insights to the catalytic mechanism. At least one magnesium ion is needed for each of the three steps of the composite ligation reaction. A two-metal model for step 1 ligase-adenylylation has been proposed, wherein one Mg^{2+} is coordinated by the β and γ phosphates of the ATP substrate and another "catalytic" Mg^{2+} engages the ATP α phosphate to stabilize the transition state of the step 1 reaction (17). The crystal structure of T4 RNA ligase 1 bound to AMPPNP and two metal ions is consistent with this idea (18). Whereas the noncatalytic Mg^{2+} is likely to exit with the PP_i leaving group after step 1 is completed, it is reasonable to think that the single catalytic metal ion remains bound to ligase and the AMP phosphate during catalysis of steps 2 and 3. The available evidence is that the catalytic metal ion is coordinated at every step by the invariant essential carboxylate side chain of motif IV (^{161}**E**GVMI in ChVLig) and, at least during steps 2 and 3, by the motif I aspartate (^{27}K*x***D**G in ChVLig) (5, 10). The motif IV Glu-161 side chain and the AMP phosphate coordinate a lutetium ion in the crystal structure of ChVLig(D29A)-AMP (6). The motif IV glutamate, the motif I aspartate, and the AMP phosphate together coordinate a zinc ion in the crystal structure of *Mycobacterium tuberculosis* LigD-AMP (19). In the crystal structure of ChVLig-AMP bound to nicked DNA, a water molecule (colored *magenta* in Fig. 1*B*) occupies the putative catalytic Mg^{2+} site, wherein it is coordinated by motif IV Glu-161, motif I Asp-29, the AMP phosphate, and the nick 3′-OH (8). Mg^{2+} in this position would be well poised to stabilize the transition state of the AMP phosphate during step 2 DNA adenylylation and to activate the 3′-OH nucleophile during step 3 phosphodiester synthesis. We were especially interested in the effects of Mg^{2+} concentration in light of the report that limiting Mg^{2+} changes the rate-limiting step for nick sealing by HuLig1 in such a way as to potentially compromise genome stability (15). It has been appreciated for more than 40 years that acidic pH conditions favor the detection of otherwise fleeting 5′-adenylylated polynucleotide species in reactions of DNA and RNA ligases at 5′-phosphate ends (20–22). Here, we conducted a systematic analysis of the effects of pH on the rates of the chemical steps that places this phenomenon on firmer mechanistic grounds.

Second, we interrogated the role of nucleotidyltransferase motif VI (located at the C terminus of the OB domain of ChVLig) during the three-step ligation pathway. Motif VI (typically R*x*DK) is a shared feature of the OB domains of ATP-dependent DNA ligases and GTP-dependent mRNA capping enzymes (Fig. 2*A*). Motif VI arginine and lysine side chains contact the β and γ phosphates of the GTP substrate in the crystal structure of *Chlorella* virus capping enzyme (Fig. 2*B*), and this interaction orients the PP_i leaving group apical to the attacking motif I lysine during the step 1 enzyme nucleotidylation reaction (23). Alanine mutations of the motif VI arginines, lysine, and aspartate residues eliminate capping enzyme activity *in vivo* (24, 25) and capping enzyme-GMP adduct formation *in vitro* (25). Although it is thought that motif VI plays an analo-

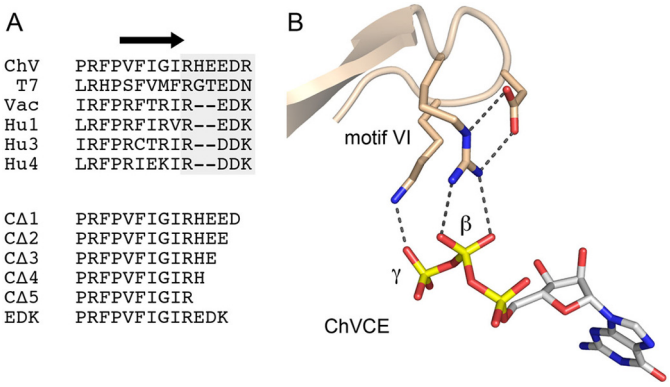

FIGURE 2. **Nucleotidyltransferase motif VI.** *A*, the amino acid sequence of motif VI (highlighted in the *shaded box*) and the preceding OB-fold β strand of *Chlorella* virus DNA ligase (*ChV*) is aligned with the corresponding segments of bacteriophage T7 (*T7*) ligase, vaccinia virus (*Vac*) ligase, human ligase I (*Hu1*), human ligase III (*Hu3*), and human ligase IV (*Hu4*). The C-terminal sequences of the ChVLig motif VI mutants studied presently are shown *below the alignment*. *B*, the figure depicts the atomic contacts of the canonical motif VI side chains with the β and γ phosphates of GTP in the crystal structure of *Chlorella* virus capping enzyme (*ChVCE*) (23).

gous role in step 1 of the DNA ligase pathway (14), no structure of a productive Lig·ATP complex is available for DNA ligases to affirm this idea. In the ChVLig-AMP and ChV-AMP-DNA crystal structures, the C-terminal residues of the motif VI peptide (which follows the last β strand of the OB domain; Fig. 2) are disordered (6, 8). Yet, we do know that the OB domain of ChVLig-AMP undergoes a large rigid-body rotation during DNA binding and clamp closure that places the C terminus (and motif VI) well away from the DNA (6–8). Motif VI is ordered and located far away from the DNA in the crystal structures of DNA-bound HuLig1 and HuLig3 (26, 27). Here, we tested a series of motif VI mutations for their impact on nick sealing by ChVLig under transient state and steady state conditions and on ligase adenylylation.

EXPERIMENTAL PROCEDURES

Recombinant ChVLig—Wild-type and mutant ChVLig proteins were produced in *Escherichia coli* and purified from soluble bacterial lysates by nickel-agarose chromatography and phosphocellulose chromatography (4). The purity and concentration of the ChVLig preparations were determined as described previously (12, 13). The detailed methods and purity data are provided in supplemental Fig. S1.

Ligase Assay—Reaction mixtures (10 μl) containing 50 mM Tris-HCl (pH 7.5), 5 mM DTT, 10 mM $MgCl_2$, 1 mM ATP, 1 pmol of ^{32}P-labeled singly nicked 36-bp duplex DNA substrate (Fig. 3; prepared as described (28)), and wild-type or mutant ChVLig as specified were incubated for 10 min at 22 °C. Single-turnover nick ligation mixtures lacked exogenous ATP. The reactions were initiated by the addition of ChVLig and quenched by the addition of 10 μl of 90% formamide, 40 mM EDTA. The samples were heated at 95 °C for 5 min. The products were resolved by electrophoresis through a 15-cm 18% polyacrylamide gel containing 7 M urea in 45 mM Tris borate, 1.25 mM EDTA. The extents of ligation were determined by scanning the gel with a Fujix BAS2500 imager. Ligation was plotted as a function of input ChVLig, with each datum being the average of three separate enzyme titration experiments. The specific activities of the wild-type and mutant ligases in ATP-dependent nick sealing were determined from the slopes of the titration curves in the linear range of enzyme dependence. The activities of the mutant ligases were normalized to the specific activity of wild-type ChVLig protein (defined as 100%) that was purified in parallel with that mutant and assayed in parallel using the same preparation of radiolabeled DNA substrate. The concentrations of preformed Lig-AMP in the enzyme preparations were determined from the slopes of the titrations curves obtained in the absence of added ATP.

Transient State Kinetic Analysis of Nick Sealing—A Kintek RQF3 rapid chemical quench apparatus was used to assay the reaction of nicked DNA with a 10-fold molar excess of preformed Lig-AMP at 22 °C in the absence of added ATP, with reaction times in the range of 0.1 to 5 s. Where applicable, longer reaction times were assayed manually. The reaction mixtures contained 50 mM Tris-HCl (pH 7.5), 5 mM DTT, 10 mM $MgCl_2$, 500 nM wild-type Lig-AMP, and 50 nM ^{32}P-5′-nick-labeled DNA substrate. The rapid kinetic measurements were initiated by mixing two solutions (20 μl each) of 50 mM Tris-HCl (pH 7.5), 5 mM DTT, 10 mM $MgCl_2$, containing 100 nM nicked DNA substrate and 1 μM ChVLig-AMP, respectively. The reactions were quenched by rapid mixing with 110 μl of 90% formamide, 50 mm EDTA. The products were analyzed by urea-PAGE, and the distribution of ^{32}P-labeled DNAs (as sealed 36-mer DNA product, 18-mer AppDNA intermediate, and residual 18-mer pDNA substrate) was quantified by scanning the gels with a Fujix BAS2500 imager.

Multiple Turnover Burst Kinetics—The reaction mixtures contained 50 mM Tris-HCl (pH 7.5), 5 mM DTT, 10 mM $MgCl_2$, 1 mM ATP, and 50 nM ^{32}P-5′-nick-labeled DNA substrate. The levels of input wild-type or mutant ChVLig were adjusted to attain 12.5 nM preformed Lig-AMP. The rapid kinetic measurements (in the range of 0.1 to 5 s) were initiated by mixing two solutions (20 μl each) of 50 mM Tris-HCl (pH 7.5), 5 mM DTT, and 10 mM $MgCl_2$ that contained 100 nM nicked DNA substrate plus 2 mM ATP (solution 1) and ChVLig (solution 2), respectively. Longer reaction times were assayed manually. Control reactions lacking ATP were performed in parallel. The products were analyzed by urea-PAGE and quantified as described above.

RESULTS AND DISCUSSION

Mg^{2+} Dependence of Rates of DNA Adenylylation and Phosphodiester Synthesis—A rapid chemical quench apparatus was used to assay the reaction of nicked DNA (Fig. 3) with a 10-fold molar excess of ChVLig-AMP in the range of 0.1 to 5 s reaction times. Longer time points were assayed manually, as warranted. Under our standard reaction conditions of 10 mM Mg^{2+}, the AppDNA intermediate peaked at 0.1 s and declined thereafter concomitant with the accumulation of the sealed DNA end product; the reaction in 10 mM Mg^{2+} was complete within 2.5 s (supplemental Fig. S2). Increasing the Mg^{2+} concentration to 20 mM or decreasing it to 5, 2, or 1 mM had little or no effect on the kinetic profile (supplemental Fig. S1). Further decrements in Mg^{2+} concentration to 0.1, 0.05, and 0.02 mM resulted in a slowing of the sealing reaction (reflected in the different *x* axis scales in the graphs in supplemental Fig. S1), but no marked change in the peak level of the AppDNA intermediate or the

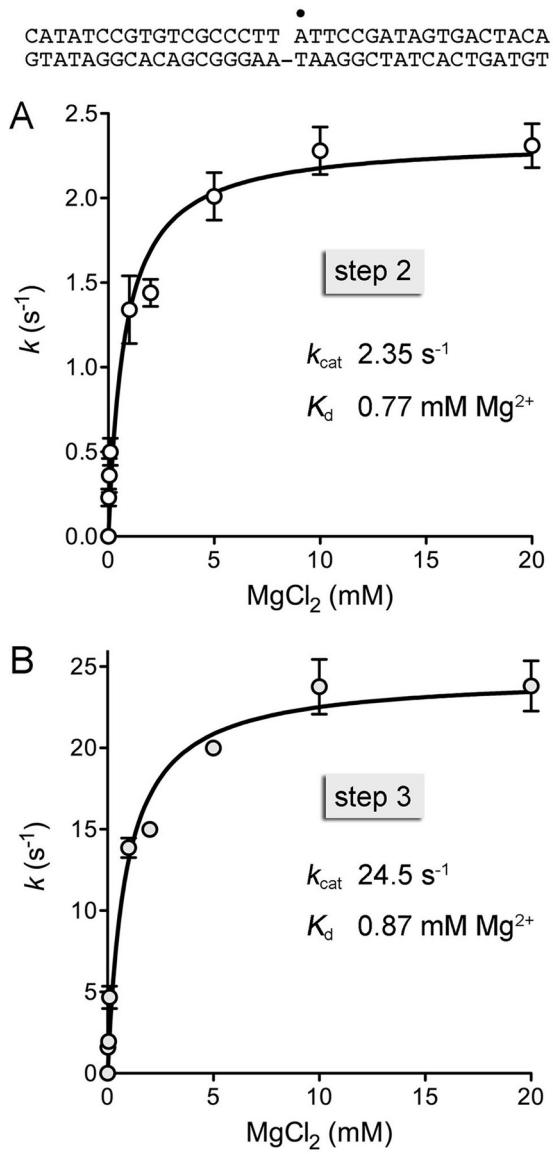

FIGURE 3. **Mg^{2+} dependence of single-turnover ligation.** The 36-bp nicked DNA substrate is depicted with the nick ^{32}P-5′-label denoted by a *filled circle*. The step 2 and step 3 rate constants and associated error values from supplemental Table S1 are plotted as a function of Mg^{2+} concentration in *A* and *B*, respectively. Nonlinear regression curve fitting of the data to a hyperbolic binding equation was executed in Prism. The k_{cat} and K_d values are indicated.

extent of nick sealing at the reaction end points (Fig. S2). By contrast, no AppDNA or sealed DNA was formed in the absence of added Mg^{2+}. The step 2 rate constants were derived from the data in supplemental Fig. S2 by fitting the kinetics of total product formation (AppDNA plus sealed DNA) to a single exponential. The step 3 rate constants (±95% confidence intervals) were calculated in MATLAB from the kinetic profiles in supplemental Fig. S2 as described (13, 14). The observed values for k_{step2} and k_{step3} are complied in supplemental Table S1 and are plotted as a function of Mg^{2+} concentration in Fig. 3*A* for step 2 and in Fig. 3*B* for step 3. Both data sets were fit well by nonlinear regression to a simple hyperbolic binding equation (Fig. 3, *A* and B) that yielded k_{step2} and k_{step3} values of 2.35 ± 0.14 s^{-1} and 24.5 ± 1.1 s^{-1}, respectively. The salient finding was that the K_d values for Mg^{2+} were nearly the same for step 2 (0.77 ± 0.22 mM Mg^{2+}) and step 3 (0.87 ± 0.19 mM Mg^{2+}). We did not observe the large disparity in step 2 and step 3 Mg^{2+} affinities reported for HuLig1 (15), whereby the step 2 K_d was 0.15 mM Mg^{2+} and the step 3 K_d was 2.6 mM Mg^{2+}. The consequence of this difference for HuLig1 is that under limiting Mg^{2+} conditions, the enzyme generates and releases high levels of AppDNA that are not sealed by HuLig1 when ATP is present (15). This low-Mg^{2+} "Achilles' heel" of the HuLig1 mechanism is apparently not shared by ChVLig. Rather, the results for ChVLig are suggestive of a common Mg^{2+} site for the DNA adenylylation and phosphodiester synthesis steps of nick sealing.

pH Dependence of Rates of Single-turnover DNA Adenylylation and Phosphodiester Synthesis—Our standard single-turnover ligation reactions are performed at pH 7.5 in 50 mM Tris-HCl buffer. Here, we varied the pH from 4.5 to 7.0 in Tris acetate buffer and from 7.0 to 9.5 in Tris-HCl buffer. The kinetic profiles are plotted in Fig. 4. It can be appreciated that raising the pH from 7.5 to 9.5 elicited a progressive but modest slowing in the rate of strand sealing, accompanied by a decrease in the peak level of the AppDNA intermediate (which comprised 2.5% of the total labeled DNA at pH 9.5), indicative of a greater impact of alkaline pH on step 2 *versus* step 3. By contrast, acidifying the pH caused a progressive and profound slowing of the overall sealing reaction (note the *x* axis scales in hundreds or thousands of seconds at pH ≤ 6.0) accompanied by accumulation of the AppDNA intermediate, to up to ~80% of the total labeled DNA at pH 4.5 to 5.0 (Fig. 4). This pattern signifies a much greater effect of acidic pH on step 3 *versus* step 2.

Plots of the log of the rate constants *versus* pH are shown in Fig. 5, *A* (step 2) and *B* (step 3). The log k_{step2} increased linearly with pH from 4.5 to 7.5, and the slope of the linear regression curve fit was 1.3, consistent with involvement of a single unprotonated functional group in step 2 catalysis that is rendered nonfunctional as it becomes protonated at acidic pH. By contrast, log k_{step3} displayed a sharper linear rise with pH from 4.5 to 7.5, and the slope of the linear regression curve fit was 2.1, suggesting involvement of two unprotonated functional groups in catalysis of the phosphodiester synthesis reaction, both of which are inactivated as they are protonated at acidic pH. On the alkaline side of the pH curve, log k_{step2} declined gradually from pH 7.5 to 9.5 with a slope of −0.6 (Fig. 5*A*), whereas log k_{step3} was flat from pH 7.5 to 9.5 (Fig. 5*B*). The steeper decrement in step 3 rate with acidic pH accounts for the transient accumulation of high levels of the AppDNA intermediate in the reactions performed at pH 4.5 to 6.5. In other words, the rate-limiting step shifts from step 2 at mildly alkaline pH (at pH 8.0, k_{step3} was 10-fold greater than k_{step2}) to step 3 at acidic pH (at pH 5.0, k_{step2} was 28-fold greater than k_{step2}).

Probing the Nature of the Protonation-sensitive Catalyst—The inflections of the log *k versus* pH curves on the acidic side suggest pK_a values in the vicinity of 7.0 for the protonation-sensitive group(s). In considering a candidate enzymic catalyst that is protonation-sensitive in this range, one would naturally focus on a histidine side chain, but this is not plausible for ChVLig, which has no histidine in or near the active site (6, 8). We deemed the metal-binding residues Glu-161 and Asp-29 as more likely prospects. To test this idea, one would, in principle,

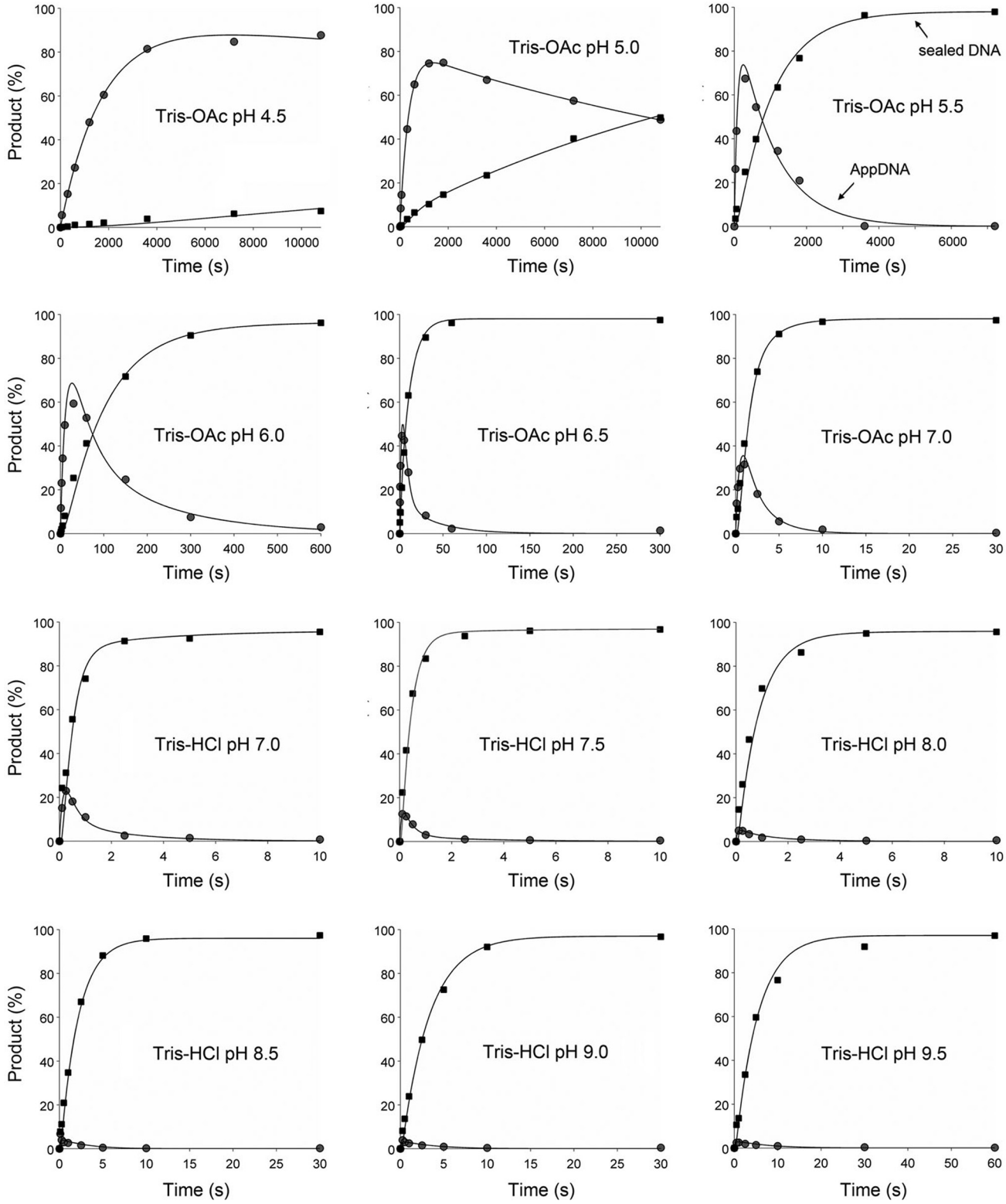

FIGURE 4. **pH dependence of the rates of single-turnover DNA adenylylation and phosphodiester synthesis.** The distributions of AppDNA intermediate (●) and sealed DNA (■) during single-turnover nick ligation at the indicated pH are plotted as a function of reaction time. Each datum in the graphs is the average of three separate kinetic experiments. The data were modeled in MATLAB (supplemental Fig. S2), and the resulting curve fits are shown.

replace Glu-161 with glutamine and Asp-29 with asparagine. Installing an isosteric amide eliminates the proton accepting ability of the native Glu and Asp groups. If either is the source of the observed acidic pH rate decrements, then we would expect the conservative amide mutants to display reduced rates of single turnover nick sealing at pH $\geq$ 7.5 (indicative of the contributions of the acidic groups to catalysis of steps 2 and 3) but not to show the additional steep rate decrements at acidic pH that

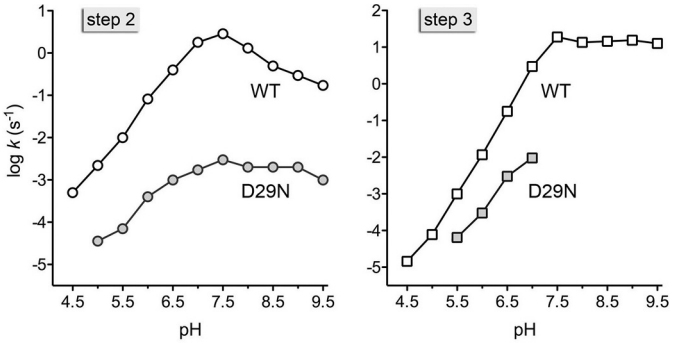

FIGURE 5. **pH-rate profiles.** *Left panel*, the step 2 rate constants for single-turnover nick sealing by wild-type (WT) ChVLig were derived from the data in Fig. 4 by fitting the kinetics of total product formation (AppDNA plus sealed DNA) to a single exponential in Prism. The pH dependence of nick sealing by the D29N mutant of ChVLig was assayed under the same conditions (not shown). The step 2 rate constants are plotted as a function of pH. *Right panel*, the step 3 rate constants for single-turnover nick sealing by WT ChVLig were calculated in MATLAB from the kinetic profiles in Fig. 4; the k_{step3} values for the D29N mutant were calculated from the respective rate profiles at pH 5.5 to 7.0 (not shown). The step 3 rate constants are plotted as a function of pH. Step 3 kinetics could not be determined for D29N at pH $\geq$ 7.5 because no AppDNA intermediate was detectable.

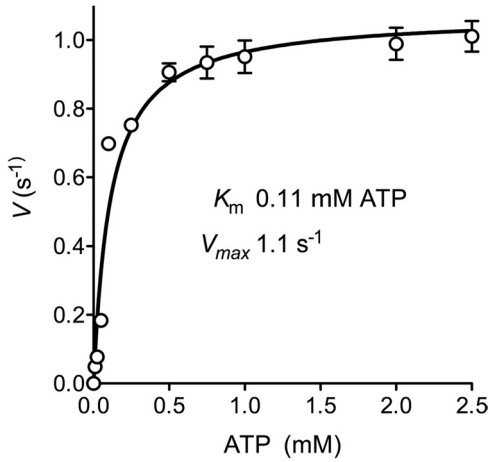

FIGURE 6. **Dependence of multiple-turnover ligation rate on ATP concentration.** Reaction mixtures containing 50 mM Tris-HCl (pH 7.5), 5 mM DTT, 10 mM $MgCl_2$, 0.1 μM ^{32}P-labeled nicked DNA substrate, 1 nM ChVLig, and ATP as specified were incubated at 22 °C. Aliquots were withdrawn at times ranging from 5 s to 15 min, and the reactions were quenched immediately with formamide/EDTA. The extents of ligation were plotted as a function of time for each ATP concentration, and the initial rates were derived by linear regression analysis in Prism. The initial rates (fmol·s^{-1}) were divided by the molar amount of input enzyme to obtain a turnover number V (s^{-1}), which is plotted in the figure as a function of ATP concentration. Each datum is the average of three separate time course experiments ± S.D. A nonlinear regression curve fit of the data to the Michaelis-Menten equation (in Prism) is shown. The K_m and V_{max} values are indicated.

were observed for wild-type ChVLig. Note that this experiment is feasible only if the conservative E161Q and D29N mutations do not affect formation of the ligase-adenylate adduct that performs single-turnover nick ligation. As reported previously (10) and verified here (data not shown), the purified recombinant E161Q protein was inactive in nick sealing or step 1 ligase adenylylation, making it impossible to study its role in step 2 catalysis.

The situation was more propitious for Asp-29, mutants of which (to Ala, Asn, or Glu) retain full activity in ligase adenylylation, are extensively preadenylylated when purified from bacteria and bind avidly to nicked DNA (5, 6, 10). Here, we purified the D29N mutant and examined its transient state kinetics as a function of pH under the same reactions conditions used to study wild-type ChVLig. The step 2 rate constants were derived by fitting the kinetics of total product formation (AppDNA plus sealed DNA) to a single exponential. A plot of the observed D29N k_{step2} values *versus* pH is shown in Fig. 5*A*. It can be readily appreciated that the D29N mutation exerted a strong negative effect on step 2 catalysis, as reflected in the downward shift in the pH rate curve by an average of 2.3 log units on the *y* axis. The salient point is that the D29N mutation did not efface the linear decline in log k_{step2} (slope of 0.81) in the pH range of 5.0 to 7.5 (Fig. 5*A*), from which we surmise that Asp-29 is not the key determinant of protonation-sensitivity during step 2 catalysis. We were able to derive D29N step 3 rate constants for the single-turnover reaction performed at pH 5.5 to 7.0, and the log k_{step3} values are plotted in Fig. 5*B*. The D29N mutations slowed the rate of step 3, as indicated by the downshift in the curve by an average of 1.3 log units compared with wild-type ChVLig. Thus, the D29N change had a milder impact on step 3 than step 2, Indeed, we were unable to determine k_{step3} for D29N at pH $>$ 7.0 because no AppDNA intermediate was detectable at any time during the reaction, signifying that under these conditions the rate of phosphodiester synthesis by D29N vastly exceeded the rate of AppDNA formation. These findings are in keeping with an earlier report that the D29N mutation did not affect the rate of phosphodiester formation at a preadenylylated DNA nick (10). The instructive point of the experiment in Fig. 5*B* is that the persistence of the acidic decrement in the step 3 rate of the D29N enzyme indicates that Asp-29 does not dictate this effect.

While arguing against Asp-29, our experiments leave open the prospect that Glu-161 is the pertinent determinant of the acid-sensitive kinetics of single-turnover nick sealing. For that to be the case, the pK_a of Glu-161 would be shifted upward to near neutrality account for the observed pH profiles. We propose an alternative explanation to account for the acid pH effect, at least on step 2 catalysis, whereby (i) the 5′-phosphate terminus of the nick is the relevant moiety that becomes protonated as the pH is lowered, and (ii) a dianionic 5′-phosphate group is necessary for productive catalysis by ligase of the attack of a 5′-phosphate oxygen on the phosphorus of Lysyl-AMP to form AppDNA. This model is consistent with the pK_a value of ~7.0 for protonation of a phosphomonoester dianion.

Steady State Kinetic Parameters—We analyzed the kinetics of nick sealing under multiple-turnover conditions in which the nicked DNA substrate was in 100-fold molar excess over the input ChVLig, and varying concentrations of ATP were included in the reaction mixtures. The initial rates were determined and are plotted in Fig. 6 as a function of ATP concentration. The data were fit by nonlinear regression to the Michaelis-Menten equation, which yielded a K_m of 0.11 ± 0.03 mM ATP and a V_{max} of 1.1 ± 0.06 s^{-1}. The turnover number under steady state conditions (which is in the same range as the single-turnover step 2 rate constant), provides a lower-bound value for the rate of ligase adenylylation.

Role of Nucleotidyltransferase Motif VI—The motif VI elements in ChVLig (RHEEDR^{298}) and bacteriophage T7 ligase

(RGTEDN) diverge by 2-amino acid insertions from the canonical R*x*DK motif VI elements found in vaccinia DNA ligase and the three human DNA ligases (Fig. 2*A*) as well as almost all other ATP-dependent DNA ligases and GTP-dependent mRNA capping enzymes. An initial study (14) showed that deleting the C-terminal ^{294}HEEDR^{298} pentapeptide of ChVLig crippled the resulting CΔ5 mutant in overall nick ligation. CΔ5 had 1% the specific activity of the wild-type enzyme and was poorly responsive to ATP. Yet, CΔ5 was active in phosphodiester synthesis at a preadenylylated nick (14). It was suggested that the CΔ5 deletion inhibited ligase adenylylation, but it remained unclear whether it also affects DNA adenylylation. To more finely probe the role of motif VI, we produced and purified a series of incremental single-amino acid C-terminal deletion mutants, named CΔ1, CΔ2, CΔ3, CΔ4, CΔ5 (Fig. 2*A*), plus an ensemble of missense mutants of the motif VI conserved residues Arg-293 and Asp-297. We also changed the motif VI sequence to a canonical element ^{293}REDK by replacing the sequence distal to Arg-293 with an "EDK" tripeptide (Fig. 2*A*).

The wild-type and mutated ChVLig proteins were produced in bacteria as N-terminal His_{10} fusions and purified from soluble bacterial extracts by nickel-agarose and phosphocellulose chromatography (supplemental Fig. S1). The extent of ligation of the nicked DNA substrate by wild-type ChVLig and each mutant was gauged as a function of input enzyme under steady state conditions in the presence of 1 mM ATP. The specific activities were calculated from the slopes of the titration curves and then normalized to the wild-type specific activity (defined as 100%). We also tested the mutants for activity *in vivo* in yeast using a plasmid shuffle assay for genetic complementation of *cdc9*Δ (7). The results are compiled in supplemental Table S2.

Subtraction of amino acids from the C terminus of ChVLig elicited progressive reductions in ligase specific activity *in vitro*, as follows: CΔ1 (34% of wild-type), CΔ2 (6%), CΔ3 (2%), CΔ4 (<1%), and CΔ5 (<1%). Replacing the deleted pentapeptide with EDK to install a consensus motif VI had no restorative effect, *i.e.* the EDK specific activity was 1% of wild-type. The CΔ4, CΔ5, and EDK mutants that were most severely crippled with respect to ligation *in vitro* were unable to complement *cdc9*Δ *in vivo* (supplemental Table S2). CΔ1, which had the highest residual activity *in vitro*, sustained wild-type growth in yeast (as gauged by colony size) at 18 and 30 °C (scored as +++ growth). However, the *ChvLIG-CΔ1* yeast strain formed smaller colonies at 37 °C (scored as ++ growth). Notwithstanding their relatively feeble nick sealing activities *in vitro*, the CΔ2 and CΔ3 mutants complemented growth of *cdc9*Δ, although in both cases, growth was slower (++) at 30 and 37 °C (supplemental Table S2). These results affirm that deletion of motif VI abolishes ChVLig activity, but they highlight that the mutational effects *in vitro* are more severe than what is reflected by *cdc9*Δ complementation. A possible basis for the *in vivo-in vitro* disparity is discussed below.

Replacing Arg-293 by alanine, lysine, and glutamine reduced ligase specific activity to 9, 13, and 13% of wild-type, respectively. Whereas R293A and R293Q were inactive in yeast, the R293K mutant supported +++ growth at 18 and 30 °C and ++ growth at 37 °C (supplemental Table S2). Thus, the positive charge at residue 293 is the pertinent requirement for activity *in vivo*. (The conundrum of this data set is that the *in vivo* "lethal" R293A and R293Q mutants have a higher specific activity *in vitro* than the *in vivo* "active" CΔ3 mutant.) Changing Asp-297 to alanine, glutamate, and asparagine lowered specific activity to 5, 10, and 2% of wild-type, respectively. D297E was active in yeast, supporting +++ growth at 18 °C and ++ growth at 30 and 37 °C. Whereas D297A was lethal, D297N allowed for very slow growth at 18 °C (yielding only pinpoint colonies, scored as +) and no growth at 30 or 37 °C (supplemental Table S2). Thus, negative charge is the relevant property at position 297. In the canonical motif VI, the putative counterparts of Arg-293 and Asp-297 form a bidentate salt bridge (Fig. 2*B*). The paradox of this data set is that changing Asp-297 to alanine eliminates activity *in vivo*, yet *in vivo* activity is preserved when the Asp-297 residue is deleted in the context of the CΔ2 or CΔ3 mutants (supplemental Table S2). A plausible explanation for this phenomenon is that the essential function of the Asp-297 side chain carboxylate can be performed by the free C-terminal main chain carboxylate of the CΔ2 or CΔ3 polypeptides.

TABLE 1
Effects of motif VI mutations on ChVLig adenylylation

ChVLig	Preformed Lig-AMP *in vivo*[a]	Lig-[^{32}P]AMP *in vitro*[b]
	% of total enzyme	*% of total enzyme*
WT	70	21
CΔ1	71	8
CΔ2	80	1.1
CΔ3	67	1.3
CΔ4	18	0.8
CΔ5	7	0.5
R293A	52	1.9
R293K	70	3.4
R293Q	48	3.8
D297A	76	2.9
D297E	74	1.8
D297N	60	2.8
EDK	53	3.6

[a] The concentrations of preformed Lig-AMP in the ChVLig preparations were determined from the slopes of the titrations profiles obtained for ATP-independent nick sealing as a function of input ChVLig.
[b] The extents of ligase adenylylation *in vitro* were calculated from the data in supplemental Fig. S3.

Effects of Motif VI Mutations on Ligase Adenylylation—Recombinant ChVLig purified from bacteria comprises a mixture of ligase apoenzyme and preformed ligase-AMP intermediate. The level of preformed Lig-AMP can be determined by assaying nick sealing in the absence of exogenous ATP, such that there is a 1:1 correspondence between the molar yield of ligated DNA and the molar amount of catalytically active Lig-AMP in the reaction. The extent of ATP-independent ligation of the singly nicked DNA substrate by wild-type ChVLig, and each mutant was gauged as a function of input enzyme. The concentrations of active Lig-AMP were calculated from the slopes of the titration curves and are expressed in Table 1 as the percent of the total enzyme comprising pre-formed Lig-AMP. In the case of wild-type ChVLig, 70% of the available enzyme was pre-adenylylated and active in single-turnover nick sealing. The levels of preformed Lig-AMP for the CΔ1 (71%), CΔ2 (80%), and CΔ3 (67%) mutants (that were active *in vivo*) were similar to that of wild-type ChVLig. By contrast, the lethal CΔ4 and CΔ5 mutants consisted of only 18 and 7% preformed Lig-AMP, respectively, signifying that the CΔ4 and CΔ5 proteins were

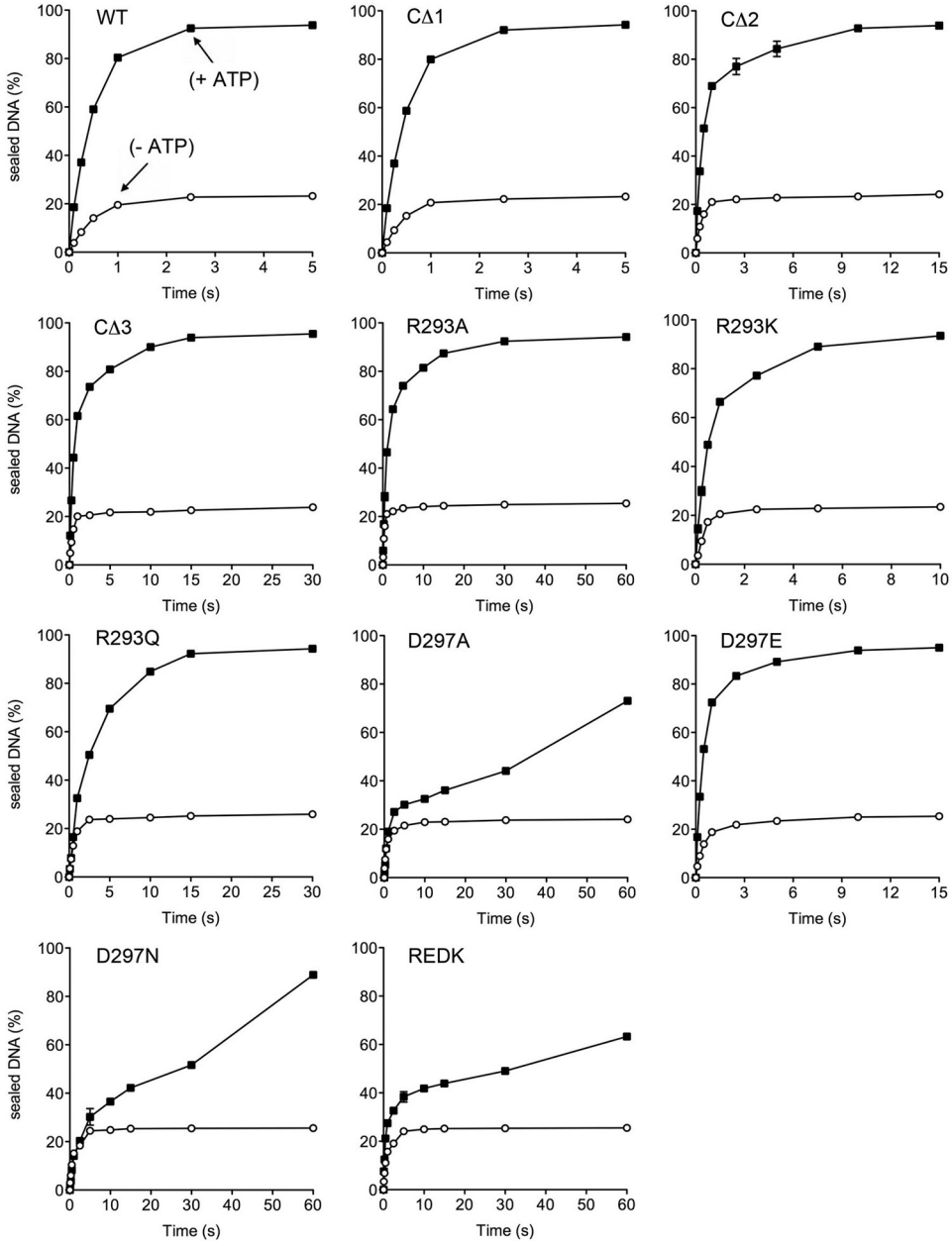

FIGURE 7. **Burst kinetics.** The extents of DNA sealing by the indicated ChVLig preparations in the presence of 1 mM ATP (■) and in the absence of ATP (○) are plotted as a function of reaction time. Each datum in the graphs is the average of three separate kinetic experiments.

defective in step 1 ligase adenylylation during their production in *E. coli*.

Reaction of ChVLig with [α-^{32}P]ATP and magnesium *in vitro* in the absence of DNA leads to the formation of a covalent LigA-[^{32}P]adenylate adduct. The autoadenylylation activities of the wild-type and mutant ChVLig preparations were assayed in parallel; the results are depicted in supplemental Fig. S3 and expressed in Table 1 as the percent of total input enzyme that was labeled *in vitro* with [^{32}P]AMP. In the case of wild-type ChVLig, 21% of the available enzyme was labeled; this value represents a labeling efficiency of 70% when corrected for the 30% fraction of the ChVLig preparation that was not preadenylylated. The CΔ1 deletion reduced the *in vitro* AMP-labeling to 8% (labeling efficiency of 20%) and the additional incremental deletions in CΔ2 and CΔ3 further suppressed *in vitro* AMP-labeling to 1.1 and 1.3%, respectively (corresponding to labeling efficiencies of 6 and 4%, respectively). The CΔ4 and CΔ5 proteins yielded 0.8 and 0.5% AMP-labeled protein, corresponding to 1 and 0.5% labeling efficiencies, respectively. Thus, effects of the motif VI deletions on the specific activity in nick sealing under steady state conditions (supplemental Table S2) correlated well with the magnitude of the defects in step 1 adenylylation activity *in vitro* (Table 1) but not necessarily with the level of adenylylation sustained *in vivo* during protein production in bacteria. This correlation also pertained to the other mutants in our collection. For example, the extents of preadenylylation of the Arg-293, Asp-297, and EDK mutants were quite high (between 48 and 76%); yet the extents of in AMP-labeling *in vitro* were consistently low (1.8% to 3.8%) and corresponded to corrected labeling efficiencies varying from 4 to 12%. This pat-

tern attests to the ability of some mutant ligases to adenylate better during their prolonged exposure to relatively high intracellular concentrations of ATP *in vivo*, *e.g.* 9.6 mM ATP in exponentially growing *E. coli* (29), compared with the 10-min reactions *in vitro* with 100 μM ATP (in the ^{32}P-AMP labeling assays) or 1 mM ATP (in the steady state nick sealing assays).

Effects of Motif VI Mutations on the Kinetics of Single-turnover Nick Sealing—The motif VI mutants for which preformed Lig-AMP comprised half or more of the enzyme preparation were selected for transient state kinetic analysis of nick sealing. The kinetic profiles are shown in supplemental Fig. S4. The step 2 and step 3 rate constants are compiled in supplemental Table S3. The CΔ1, CΔ2, and CΔ3 truncations and the various Arg-293 and Asp-297 mutations had little or no effect on the rates of DNA adenylylation or phosphodiester synthesis by the preadenylylated ligases. The EDK mutation elicited only a modest (2-fold) reduction in both rates. Therefore, we conclude that motif VI is dispensable for the steps of the ligation pathway subsequent to ligase adenylylation.

Burst Kinetics Highlight the Role of Motif VI in Ligase Adenylylation—We investigated the kinetics of nick joining by wild-type ChVLig and selected motif VI mutants in the presence and absence of 1 mM ATP under conditions in which the nicked DNA substrate was in ~4-fold molar excess over preformed Lig-AMP. In the reactions lacking ATP, each enzyme executed a single round of sealing of 20–25% of the input DNA substrate within 1 to 5 s (Fig. 7, *open circles*). Because the wild-type enzyme preparation is a mixture of Lig-AMP and apoLig, we anticipated that inclusion of ATP would not only increase the reaction end point, by allowing multiple rounds of sealing, but that the initial rate of the reaction might also be enhanced because the apoLig can react with ATP to form additional Lig-AMP, provided that the rate of ligase adenylylation (step 1) was comparable with or faster than the rate of DNA adenylylation (step 2). This scenario was borne out for wild-type ChVLig (Fig. 7, *top left graph*). However, if a mutation exerts a negative effect on the rate of ligase adenylylation, such that it becomes slower than the rate of DNA adenylylation, then we would expect to observe a pattern of burst kinetics in the presence of ATP, whereby the preformed mutant Lig-AMP rapidly seals a stoichiometric amount of the input nicks (similar to the −ATP reaction), followed by a slow phase of steady state nick sealing, the relative rate of which is reflective of the ligase adenylylation step. Indeed, we observed burst kinetics profiles for the D297A, D297N, and EDK mutants (Fig. 7).

By plotting the different between the extents of sealing in the +ATP and −ATP reactions as a function of time, and calculating the slope of the linear phase of the curve (supplemental Fig. S5), we could infer the relative rates of ligase-adenylation at 1 mM ATP concentration. The key points are as follows. The D297A and D297N mutations depressed the slope by two orders of magnitude, whereas D297E was nearly as responsive to ATP as wild-type, thereby underscoring the essentiality of the 297 side chain carboxylate for ligase adenylylation. The CΔ2 and CΔ3 mutants that lack Asp-297 were almost as responsive to ATP as wild-type ChVLig and D297E, consistent with the free C-terminal main-chain 296 carboxylate filling in for the 297 side chain carboxylate during ligase adenylylation. The hierarchy of effects on ATP responsiveness of Arg-293 mutants underscores the importance of positive charge at this position. Also, it is noteworthy that the D297A and D297N mutations have a relatively greater impact on ATP responsiveness than R293A and R293Q (supplemental Fig. S5), which suggests that Asp-297 plays a more prominent role in step 1 ligase adenylylation than the "structural" role in tethering the motif VI arginine suggested by the structure of *Chlorella* virus capping enzyme (Fig. 2*B*). It is conceivable that Asp-297 in the noncanonical motif VI of ChVLig might be a component of the coordination complex of the "noncatalytic" Mg^{2+} that is proposed to bind the ATP β and γ phosphates.

In conclusion, our kinetic analysis of ChVLig provides new insights to catalysis by ATP-dependent DNA ligases by illuminating the following: (i) the distinct responses of the rates of DNA adenylylation and phosphodiester synthesis to pH, such that the latter becomes rate-limiting under acidic conditions; (ii) the potential role of the ionization state of the nick 5′-phosphate as a determinant of the rate of DNA adenylylation; (iii) the nearly equivalent binding affinities of ChVLig for Mg^{2+} during steps 2 and 3, a feature that distinguishes ChVLig from HuLig1; and (iv) the catalytic contributions of motif VI, especially the Asp-297 carboxylate, exclusively during the ligase adenylylation step.

REFERENCES

1. Lehman, I. R. (1974) DNA ligase: Structure, mechanism, and function. *Science* **186,** 790–797
2. Ellenberger, T., and Tomkinson, A. E. (2008) Eukaryotic DNA ligases: Structural and functional insights. *Annu. Rev. Biochem.* **77,** 313–338
3. Ho, C. K., Van Etten, J. L., and Shuman, S. (1997) Characterization of an ATP-dependent DNA ligase encoded by *Chlorella* virus PBCV-1. *J. Virol.* **71,** 1931–1937
4. Sriskanda, V., and Shuman, S. (1998) *Chlorella* virus DNA ligase: Nick recognition and mutational analysis. *Nucleic Acids Res.* **26,** 525–531
5. Odell, M., and Shuman, S. (1999) Footprinting of *Chlorella* virus DNA ligase bound at a nick in duplex DNA. *J. Biol. Chem.* **274,** 14032–14039
6. Odell, M., Sriskanda, V., Shuman, S., and Nikolov, D. (2000) Crystal structure of eukaryotic DNA ligase-adenylate illuminates the mechanism of nick sensing and strand joining. *Mol. Cell* **6,** 1183–1193
7. Odell, M., Malinina, L., Sriskanda, V., Teplova, M., and Shuman, S. (2003) Analysis of the DNA joining repertoire of *Chlorella* virus DNA ligase and a new crystal structure of the ligase-adenylate intermediate. *Nucleic Acids Res.* **31,** 5090–5100
8. Nair, P. A., Nandakumar, J., Smith, P., Odell, M., Lima, C. D., and Shuman, S. (2007) Structural basis for nick recognition by a minimal pluripotent DNA ligase. *Nat. Struct. Mol. Biol.* **14,** 770–778
9. Shuman, S., and Lima, C. D. (2004) The polynucleotide ligase and RNA capping enzyme superfamily of covalent nucleotidyltransferases. *Curr. Opin. Struct. Biol.* **14,** 757–764
10. Sriskanda, V., and Shuman, S. (2002) Role of nucleotidyltransferase motifs I, III and IV in the catalysis of phosphodiester bond formation by *Chlorella* virus DNA ligase. *Nucleic Acids Res.* **30,** 903–911
11. Sriskanda, V., and Shuman, S. (2002) Role of nucleotidyl transferase motif V in strand joining by *chlorella* virus DNA ligase. *J. Biol. Chem.* **277,** 9661–9667
12. Samai, P., and Shuman, S. (2011) Functional dissection of the DNA interface of the nucleotidyltransferase domain of *Chlorella* virus DNA ligase. *J. Biol. Chem.* **286,** 13314–13326
13. Samai, P., and Shuman, S. (2011) Structure-function analysis of the OB and latch domains of *Chlorella* virus DNA ligase. *J. Biol. Chem.* **286,** 22642–22652
14. Sriskanda, V., and Shuman, S. (1998) Mutational analysis of *Chlorella* virus DNA ligase: Catalytic roles of domain I and motif VI. *Nucleic Acids*

Res. **26,** 4618–4625
15. Taylor, M. R., Conrad, J. A., Wahl, D., and O'Brien, P. J. (2011) Kinetic mechanism of human DNA ligase I reveals magnesium-dependent changes in the rate-limiting step that compromise ligation efficiency. *J. Biol. Chem.* **286,** 23054–23062
16. Lohman, G. J., Chen, L., and Evans, T. C., Jr. (2011) Kinetic characterization of single strand break ligation in duplex DNA by T4 DNA ligase. *J. Biol. Chem.* **286,** 44187–44196
17. Cherepanov, A. V., and de Vries, S. (2002) Kinetic mechanism of the Mg^{2+}-dependent nucleotidyl transfer catalyzed by T4 DNA and RNA ligases. *J. Biol. Chem.* **277,** 1695–1704
18. El Omari, K., Ren, J., Bird, L. E., Bona, M. K., Klarmann, G., LeGrice, S. F., and Stammers, D. K. (2006) Molecular architecture and ligand recognition determinants for T4 RNA ligase. *J. Biol. Chem.* **281,** 1573–1579
19. Akey, D., Martins, A., Aniukwu, J., Glickman, M. S., Shuman, S., and Berger, J. M. (2006) Crystal structure and nonhomologous end-joining function of the ligase component of mycobacterium DNA ligase D. *J. Biol. Chem.* **281,** 13412–13423
20. Harvey, C. L., Gabriel, T. F., Wilt, E. M., and Richardson, C. C. (1971) Enzymatic breakage and joining of deoxyribonucleic acid. IX. Synthesis and properties of the deoxyribonucleic acid adenylate in the phage T4 ligase reaction. *J. Biol. Chem.* **246,** 4523–4530
21. Ho, C. K., and Shuman, S. (2002) Bacteriophage T4 RNA ligase 2 (gp24.1) exemplifies a family of RNA ligases found in all phylogenetic domains. *Proc. Natl. Acad. Sci. U.S.A.* **99,** 12709–12714
22. Yin, S., Kiong Ho, C., Miller, E. S., and Shuman, S. (2004) Characterization of bacteriophage KVP40 and T4 RNA ligase 2. *Virology* **319,** 141–151
23. Håkansson, K., Doherty, A. J., Shuman, S., and Wigley, D. B. (1997) X-ray crystallography reveals a large conformational change during guanyl transfer by mRNA capping enzymes. *Cell* **89,** 545–553
24. Wang, S. P., Deng, L., Ho, C. K., and Shuman, S. (1997) Phylogeny of mRNA capping enzymes. *Proc. Natl. Acad. Sci. U.S.A.* **94,** 9573–9578
25. Sawaya, R., and Shuman, S. (2003) Mutational analysis of the guanylyltransferase component of mammalian mRNA capping enzyme. *Biochemistry* **42,** 8240–8249
26. Pascal, J. M., O'Brien, P. J., Tomkinson, A. E., and Ellenberger, T. (2004) Human DNA ligase I completely encircles and partially unwinds nicked DNA. *Nature* **432,** 473–478
27. Cotner-Gohara, E., Kim, I. K., Hammel, M., Tainer, J. A., Tomkinson, A. E., and Ellenberger, T. (2010) Human DNA ligase III recognizes DNA ends by dynamic switching between two DNA-bound states. *Biochemistry* **49,** 6165–6176
28. Shuman, S. (1995) Vaccinia virus DNA ligase: Specificity, fidelity, and inhibition. *Biochemistry* **34,** 16138–16147
29. Bennett, B. D., Kimball, E. H., Gao, M., Osterhout, R., Van Dien, S. J., and Rabinowitz, J. D. (2009) Absolute metabolite concentrations and implied enzyme active site occupancy in *Escherichia coli*. *Nat. Chem. Biol.* **5,** 593–599